

23. Prialnik, D. & Kovetz, A. An extended grid of multicycle nova evolution models. *Astrophys. J.* **445**, 789–810 (1995).
24. Soker, N. & Tylenda, R. Main-sequence stellar eruption model for V838 Monocerotis. *Astrophys. J.* **582**, L105–L108 (2003).
25. Iben, I. & Tutukov, A. V. Rare thermonuclear explosions in short-period cataclysmic variables, with possible application to the nova-like red variable in the Galaxy M31. *Astrophys. J.* **389**, 369–374 (1992).
26. Goranskii, V. P. *et al.* Nova Monocerotis 2002 (V838 Mon) at early outburst stages. *Astron. Lett.* **28**, 691–700 (2002).
27. Osiwala, J. P. *et al.* The double outburst of the unique object V838 Mon. in *Symbiotic Stars Probing Stellar Evolution* (eds Corradi, R. L. M., Mikolajewska, J. & Mahoney, T. J.) (ASP Conference Series, San Francisco, in the press).
28. Price, A. *et al.* Multicolor observations of V838 Mon. *IAU Inform. Bull. Var. Stars* **5315**, 1 (2002).
29. Crause, L. A. *et al.* The post-outburst photometric behaviour of V838 Mon. *Mon. Not. R. Astron. Soc.* (in the press).

Acknowledgements This Letter is based on observations with the NASA/ESA Hubble Space Telescope, obtained at the Space Telescope Science Institute, which is operated by AURA, Inc. under a NASA contract. We thank the Space Telescope Science Institute for awarding Director's Discretionary Observing Time for this project, and for support. S.S. was supported, in part, by NSF and NASA grants to Arizona State University.

Competing interests statement The authors declare that they have no competing financial interests.

Correspondence and requests for materials should be addressed to H.E.B. (e-mail: bond@stsci.edu).

Realization of the Cirac–Zoller controlled-NOT quantum gate

Ferdinand Schmidt-Kaler, Hartmut Häffner, Mark Riebe, Stephan Gulde, Gavin P. T. Lancaster, Thomas Deuschle, Christoph Becher, Christian F. Roos, Jürgen Eschner & Rainer Blatt

Institut für Experimentalphysik, Universität Innsbruck, Technikerstraße 25, A-6020 Innsbruck, Austria

Quantum computers have the potential to perform certain computational tasks more efficiently than their classical counterparts. The Cirac–Zoller proposal¹ for a scalable quantum computer is based on a string of trapped ions whose electronic states represent the quantum bits of information (or qubits). In this scheme, quantum logical gates involving any subset of ions are realized by coupling the ions through their collective quantized motion. The main experimental step towards realizing the scheme is to implement the controlled-NOT (CNOT) gate operation between two individual ions. The CNOT quantum logical gate corresponds to the XOR gate operation of classical logic that flips the state of a target bit conditioned on the state of a control bit. Here we implement a CNOT quantum gate according to the Cirac–Zoller proposal¹. In our experiment, two ⁴⁰Ca⁺ ions are held in a linear Paul trap and are individually addressed using focused laser beams²; the qubits³ are represented by superpositions of two long-lived electronic states. Our work relies on

recently developed precise control of atomic phases⁴ and the application of composite pulse sequences adapted from nuclear magnetic resonance techniques^{5,6}.

Any implementation of a quantum computer (QC) has to fulfil a number of essential criteria (summarized in ref. 7). These criteria include: a scalable physical system with well characterized qubits, the ability to initialize the state of the qubits, long relevant coherence times (much longer than the gate operation time), a qubit-specific measurement capability and a ‘universal’ set of quantum gates. A QC can be built using single qubit operations (‘rotations’) and two-qubit CNOT gates because any computation can be decomposed into a sequence of these basic gate operations^{8,9}. So far, quantum algorithms have been implemented only with nuclear magnetic resonance (NMR) and ion trap systems. Recently, using NMR techniques, complex quantum algorithms such as Shor’s factorizing algorithm¹⁰ employing seven qubits have been demonstrated¹¹. In NMR systems qubits are encoded in mixed states and ensemble measurements reveal the computational output. Thus, NMR implementations of a QC are not scalable in principle, although they provide an ideal system for testing procedures and algorithms.

In contrast, trapped ions allow one to prepare and manipulate pure states such that quantum computation is scalable. In addition, cooled, trapped ions exhibit unique features which make them ideally suited for implementations of a QC¹². In particular, their quantum state of motion can be controlled to the zero point of the trapping potential^{13,14}, they provide a long time for manipulations of the qubits¹³ encoded in long-lived internal states³, and their quantum state can be detected with efficiencies close to 100% (ref. 15). During the past years two and four ions have been entangled^{16,17}, a single-ion CNOT gate¹⁸ has been realized, and recently the Deutsch–Jozsa algorithm¹⁹ has been implemented on a single-ion quantum processor. While the entangling operations demonstrated in ref. 17 can be used as a logic gate, a two-ion gate using individual addressing has not been demonstrated. This may serve as a key element for the further development and future perspectives towards general purpose quantum computing with trapped ions.

To implement a QC, Cirac and Zoller proposed a string of ions in a linear trap to serve as a quantum memory where the qubit information is carried by two internal states of each ion. Computational operations are carried out by addressing the ions individually with a laser beam. Single-qubit rotations are performed using coherent excitation by a single laser pulse driving transitions between the qubit states. For a two-qubit CNOT operation, Cirac and Zoller proposed to use the common vibration of an ion string to convey the information for a conditional operation (this vibrational mode is called the ‘bus-mode’). This can be achieved with a sequence of three steps after the ion string has been prepared in the ground state $\langle n = 0 \rangle$ of the bus-mode. First, the quantum information of the control ion is mapped onto this vibrational mode, that is, the entire string of ions is moving and thus the target ion participates in this common motion. Second, and conditional upon the motional state, the target ion’s qubit is inverted. Finally, the state of the bus-mode is mapped back onto the control ion. Mathematically, this amounts to performing the operation

Table 1 Pulse sequence for the Cirac–Zoller CNOT quantum gate operation

Ion 1	Ion 2	Ion 2	Ion 2	Ion 1
$R_1^+(\pi, 0)$ Mapping	$R_2(\pi/2, 0)$ Ramsey	$R_2^+(\pi, 0)$	$R_2^+(\pi/\sqrt{2}, \pi/2)$ Composite single ion phase gate	$R_2^+(\pi/\sqrt{2}, \pi/2)$
				$R_2(\pi/2, \pi)$ Ramsey ⁻¹
				$R_1^+(\pi, \pi)$ Mapping ⁻¹

$R_j(\theta, \varphi)$, $R_j^+(\theta, \varphi)$ denote transitions on the carrier and the blue sideband, respectively, for the j th ion. θ denotes the angle of the rotation, defined by the Rabi frequency and the pulse length; φ denotes the axis of the rotation, given by the phase between the exciting radiation and the atomic polarization.

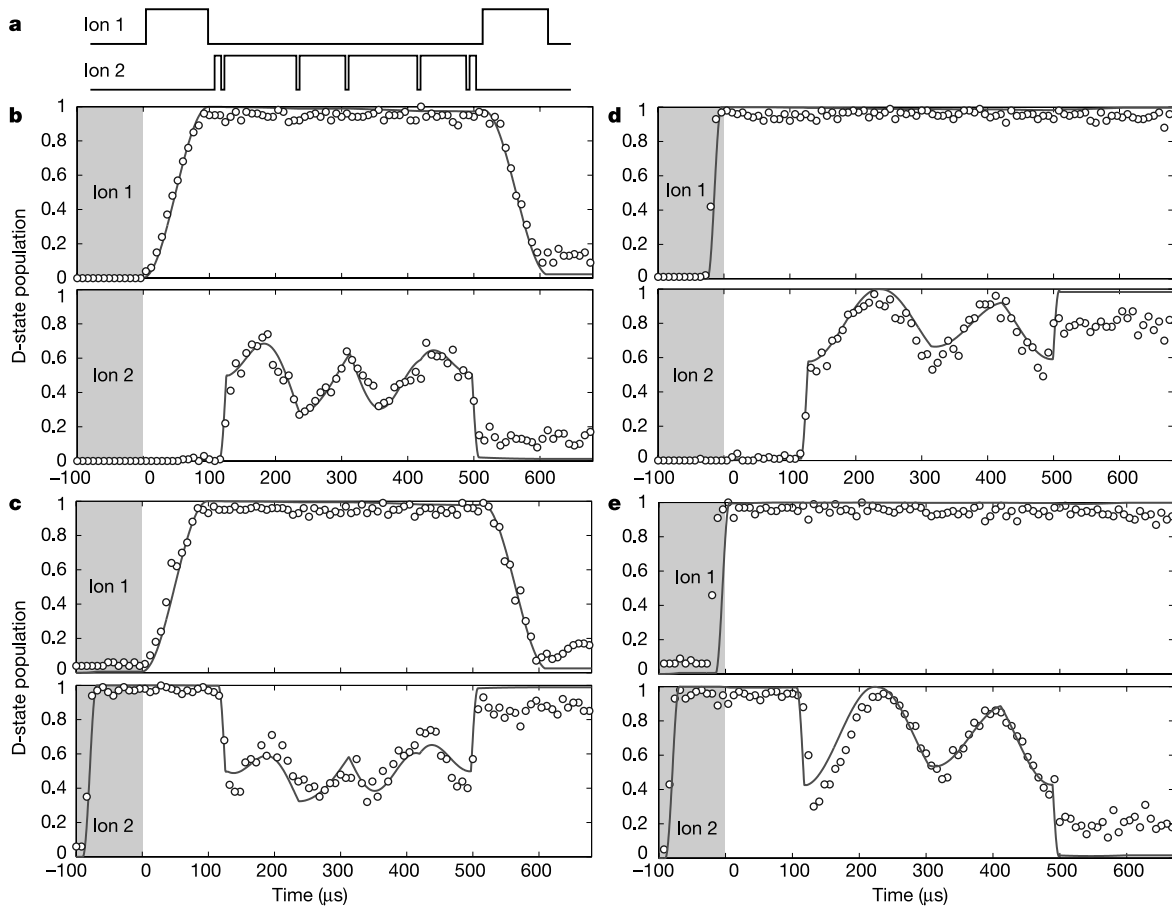


Figure 1 State evolution of both qubits under the CNOT operation. For this, the pulse sequence (a) (see also Table 1) is truncated as a function of time and the $D_{5/2}$ state probability is measured (b–e). The solid lines indicate the theoretically expected behaviour. They do not represent a fit. Input parameters for the calculations are the independently measured Rabi frequencies on the carrier and sideband transitions and the addressing error. The initial state preparation is indicated by the shaded area and drawn in

all figures for negative time values. The actual Cirac–Zoller CNOT gate pulse sequence starts at $t = 0$. After mapping the first ion’s state (control qubit) with a π -pulse of length $95 \mu\text{s}$ to the bus-mode, the single-ion CNOT sequence (consisting of six concatenated pulses) is applied to the second ion (target qubit) for a total time of $380 \mu\text{s}$. Finally, the control qubit is reset to its original value with the concluding π -pulse applied to the first ion for $95 \mu\text{s}$.

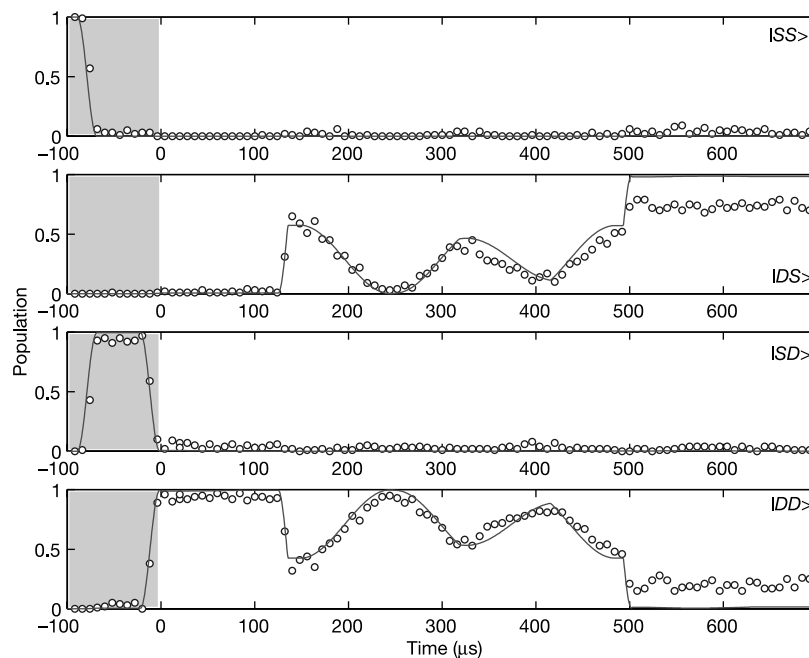


Figure 2 Joint probabilities for the ions prepared in $|DD\rangle$. The data points represent the probability for the ion string to be in the state indicated on the right-hand side. Shaded

areas represent the preparation period. The measurement procedure is the same as in Fig. 1.

Table 2 **Error budget**

Error source	Magnitude	Contribution
Laser frequency noise (phase coherence)	~100 Hz (FWHM)	10%
Laser intensity fluctuations	~3% peak to peak	~1%
Laser detuning error	~200 Hz	~2%
Residual thermal excitation	$\langle n \rangle_{\text{bus}} < 0.02$ $\langle n \rangle_{\text{other}} < 6$	2% 0.4%
Addressing error	5% in Rabi frequency (at neighbouring ion)	3%
Off-resonant excitations	for $t_{\text{gate}} = 600 \mu\text{s}$	4%
Total contribution of error sources		~20%

The errors accounted for in our experimental apparatus are specified. Laser frequency and intensity noise occurs as a result of imperfect laser stabilization. Slow drift of the laser locking cavity gives rise to detuning errors. Residual thermal excitation of the bus-mode results from non-optimal sideband cooling. The finite width of the focused laser beam at the position of the ion string produces residual excitation at the site of the non-addressed ion. The intense laser light applied on the blue sideband transitions produces off-resonant carrier excitations. The contributions to the loss of fidelity are calculated from the magnitude of errors occurring from each source. As can be seen from the table, the imperfect locking of our laser is responsible for the majority of the error budget. The individual errors are considered to be independent, the total error results from calculating the success probability given by $\prod_i(1 - \epsilon_i)$, where the ϵ_i are given by the individual errors below.

$|\epsilon_1\rangle|\epsilon_2\rangle \rightarrow |\epsilon_1\rangle|\epsilon_1 \oplus \epsilon_2\rangle$ with $\epsilon_{1,2} \in \{0, 1\}$ describing the logical state of the two qubits in question and \oplus denoting addition modulo 2. Thus, the CNOT gate operation is described by the unitary operation:

$$\begin{array}{cccc}
 & |00\rangle & |01\rangle & |10\rangle & |11\rangle \\
 \begin{array}{c} |00\rangle \\ |01\rangle \\ |10\rangle \\ |11\rangle \end{array} & \begin{pmatrix} 1 & 0 & 0 & 0 \\ 0 & 1 & 0 & 0 \\ 0 & 0 & 0 & 1 \\ 0 & 0 & 1 & 0 \end{pmatrix} & & &
 \end{array} \quad (1)$$

where the input and output states of the two qubits $|\epsilon_1\rangle|\epsilon_2\rangle = |\epsilon_1\epsilon_2\rangle$ are encoded by the electronic states of the ions.

For the experimental implementation we load two $^{40}\text{Ca}^+$ ions into a linear Paul trap. We encode a qubit in a superposition of the $S_{1/2}$ ground state and metastable $D_{5/2}$ state (lifetime $\tau \approx 1\text{ s}$)¹⁹ according to $S_{1/2} \rightarrow |0\rangle$ and $D_{5/2} \rightarrow |1\rangle$. The qubits are manipulated on the $S_{1/2}$ to $D_{5/2}$ quadrupole transition near 729 nm, using a narrowband Ti:sapphire laser (bandwidth $< 100\text{ Hz}$, relative intensity noise $< 0.02_{\text{r.m.s.}}$) which is tightly focused onto individual ions in the string. An electro-optical beam deflector switches the beam between the ions. We measure the qubit by an electron shelving technique^{13,15}. For details on the individual state manipulation and detection see the Methods. We start the experimental cycle by Doppler cooling³ for 2 ms. Using sympathetic sideband cooling²⁰ for 8 ms we prepare the bus-mode (breathing mode at $\omega_b = 2\pi \times 2.1\text{ MHz}$) in $|n=0\rangle$, achieving about 99% ground state occupation. The ions' electronic qubit states are initialized by optical pumping¹⁹.

Qubit manipulations required for the CNOT operation are realized by applying laser pulses with well-defined phases on the 'carrier' or the 'blue sideband' of the electronic quadrupole transition as described in the Methods and listed in Table 1. Note throughout the following that we always perform sideband pulses on the blue sideband. For the gate sequence, first a π -pulse applied to the blue sideband of the first ion (that is, the control qubit) maps its internal state to a corresponding state of the bus-mode. The phonon-number, n , of the bus-mode also forms a qubit where $|n=0\rangle$ ($|n=1\rangle$) represents the logical state $|1\rangle$ ($|0\rangle$)¹⁹. With the quantum information of the control qubit in the vibrational mode, we address the second ion (that is, the target qubit) and perform a single-ion CNOT gate operation between this ion and the bus-mode. The second ion's internal state is flipped if no vibration is present in the bus-mode, that is, if the bus-qubit is $|1\rangle$. This

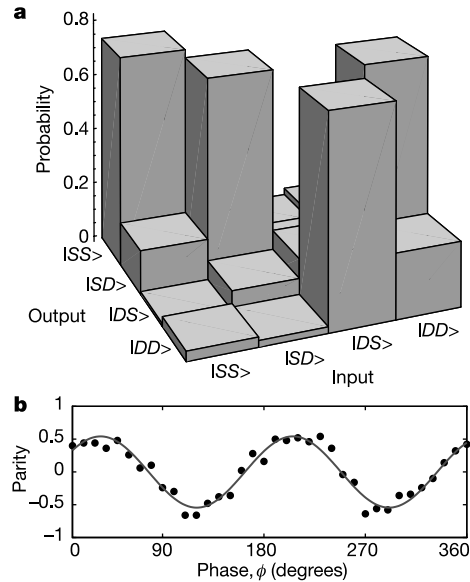


Figure 3 Cirac-Zoller CNOT gate operation. **a**, Experimentally observed truth table of the Cirac-Zoller CNOT operation derived from joint-probability measurements as in Fig. 2. Ideally, the table should reproduce the squared moduli of the entries of the unitary operation given in equation (1). Experimentally, we find that the currently available fidelity of the gate operation is limited to about 70–80%; detailed values of measured probabilities are listed below:

	$ SS\rangle$	$ SD\rangle$	$ DS\rangle$	$ DD\rangle$
$ SS\rangle$	0.74(3)	0.13(3)	0.05(3)	0.08(3)
$ SD\rangle$	0.15(3)	0.71(5)	0.06(1)	0.08(2)
$ DS\rangle$	0.01(2)	0.08(3)	0.14(4)	0.77(3)
$ DD\rangle$	0.03(3)	0.02(1)	0.72(6)	0.22(4)

b, Cirac-Zoller gate operation with a superposition $1/\sqrt{2}(|S\rangle + |D\rangle)|S\rangle$ as input results in an entangled output state $1/\sqrt{2}(|SS\rangle + e^{i\phi}|DD\rangle)$. We analyse the entanglement by applying $\pi/2$ -pulses with phase ϕ to both ions after the gate operation and by measuring the parity¹⁷ $P = P_{SS} + P_{DD} - (P_{SD} + P_{DS})$ as a function of the phase ϕ (P_{ij} denotes the probability to find the ions in the states $|ij\rangle$, $i, j = S$ or D). The quantum nature of the gate operation is proved by observing oscillations with $\cos(2\phi)$, whereas a non-entangled state would yield a variation with $\cos(\phi)$ only. From the observed visibility of 0.54(3) and the observed populations $P_{SS} = 0.42(3)$ and $P_{DD} = 0.45(3)$ prior to the analysing pulses we calculate¹⁷ a fidelity of $F = 0.71(3)$.

operation consists of a pair of Ramsey pulses enclosing a composite phase gate¹⁹; for details see the Methods. Finally, a π -pulse on the blue sideband applied to the first ion restores the controlling qubit and the bus-mode to their original states. The pulse sequence applied to ions 1 and 2 is sketched in Fig. 1a. The composite pulse sequence replaces the 2π -rotation on an auxiliary transition as originally proposed by Cirac and Zoller¹.

The two ions are prepared in their respective eigenstates, that is, in either the $|\epsilon_i\rangle = |S\rangle \equiv |0\rangle$ or $|\epsilon_i\rangle = |D\rangle \equiv |1\rangle$ states using single qubit rotations. In order to trace the state of both qubits under the CNOT operation, we truncate the CNOT pulse sequence at a certain time and measure the probability of finding the ions in the $D_{5/2}$ state. In Fig. 1b–e we display this probability as a function of time for all four initial settings $|\epsilon_1\rangle|\epsilon_2\rangle = |\epsilon_1\epsilon_2\rangle = |SS\rangle, |SD\rangle, |DS\rangle, |DD\rangle$. As shown in Fig. 1, the state evolution of ion 2 follows trajectories depending on the initially prepared qubit states of ion 1. The data agree well with the calculated ideal evolution (given by the solid lines in Fig. 1, no fit parameters). The outcome of the gate operation is inferred from the measured state after the final pulse and it proves

that the second ion's internal state is flipped when the first ion was prepared in the $|D\rangle$ state (see Fig. 1d, e), whereas it remains in its original state if the first ion was prepared in the $|S\rangle$ state (see Fig. 1b, c).

In a second experiment, we measured independently for each time step the joint probability of finding the ions in either the $|SS\rangle$, $|SD\rangle$, $|DS\rangle$ or $|DD\rangle$ state. Such a joint-probability measurement is displayed in Fig. 2 for the case of the ions starting in the $|DD\rangle$ state. From these measurements we derived the truth table graphically shown in Fig. 3a. The fidelity of transferring the initially prepared eigenstates into the final target states is optimally 80%; the fidelity of creating an entangled state is $F = 0.71(3)$, as shown in Fig. 3b.

The performance of this CNOT gate operation is currently limited by a number of technical shortcomings which are listed in Table 2. The observed fidelity is well understood from these limitations. It is to be expected that technical improvements such as reduction of laser frequency noise and improved control of the addressing beam will allow us to further increase the fidelity to more than 90% in the near future. Still higher fidelities will require more complex composite pulse techniques²¹ and/or quantum control techniques²² which take full account of the experimental imperfections, for example the residual thermal excitation and inaccuracies in the pulse shaping. Eventually, and in order to overcome decoherence for longer pulse sequences, the qubits will have to be encoded in hyperfine states of ions less susceptible to environmental influences, such as $^{43}\text{Ca}^+$ ions.

These results demonstrate the feasibility and the flexibility of ion trap QC technology. This will provide the basis for experiments using operations between few qubits, as are needed, for example, for the preparation of Bell and GHZ states²³ with ions, for implementing error correction protocols²⁴, and for applications with quantum repeaters²⁵. □

Methods

Level scheme and state manipulation

Quantum information is encoded in trapped Ca^+ ions employing the electronic $|S_{1/2}, m_j = -1/2\rangle$ and $|D_{3/2}, m_j = -1/2\rangle$ levels of a narrow quadrupole transition³ near 729 nm. The ions are prepared in the ground state of the trap's harmonic oscillator potential by laser cooling¹³. Manipulation of the internal qubit state is performed by exciting the ion on the $|S_{1/2}\rangle - |D_{3/2}\rangle$ resonance ('carrier') transition while the vibrational degrees of freedom are manipulated on the 'blue detuned sideband', that is, on a transition which changes both the electronic and motional degrees of freedom¹⁹.

In order to switch between carrier (R) and sideband (R⁺) rotations we shift the laser frequency with an acousto-optical modulator¹⁹. The phase of the light field is controlled via the phase of the radio frequency driving the acousto-optical modulator with an accuracy of 0.06 rad. Additional phase shifts due to light shifts arise because we have to drive sideband transitions (which couple much more weakly than carrier transitions) with high laser intensity. We cancel the unwanted light shifts with an additional off-resonant laser field inducing a light shift of equal strength but opposite sign⁴.

Phase gate and CNOT gate operations which change the electronic state of a single ion conditional upon the state of motion have been implemented previously using composite pulse techniques¹⁹. For an implementation of the single-ion CNOT gate operation we use a combination of a pair of Ramsey pulses and a phase gate operation. The computational subspace for this operation consists of the states $|S,0\rangle$, $|D,0\rangle$, $|S,1\rangle$, $|D,1\rangle$, that is the electronic states of the ion ($|S\rangle$, $|D\rangle$) and the phonon state ($|n=0\rangle$, $|n=1\rangle$). The matrix describing the phase gate operation is given by:

$$\begin{matrix} |S, n=1\rangle & |D, n=1\rangle & |S, n=0\rangle & |D, n=0\rangle \\ \begin{pmatrix} |S, n=1\rangle \\ |D, n=1\rangle \\ |S, n=0\rangle \\ |D, n=0\rangle \end{pmatrix} & \begin{pmatrix} -1 & 0 & 0 & 0 \\ 0 & -1 & 0 & 0 \\ 0 & 0 & -1 & 0 \\ 0 & 0 & 0 & 1 \end{pmatrix} & & (2) \end{matrix}$$

With a 2π -rotation on the blue sideband the $|S,0\rangle$ and $|D,1\rangle$ state amplitudes acquire a phase factor of -1 . The state $|D,0\rangle$ is not affected by this operation and its phase does not change. However, transitions starting from the $|S,1\rangle$ state would yield a rotation of $2\pi\sqrt{2}$ because the sideband Rabi frequency depends on the phonon number. This shortcoming can be circumvented by using a combination of four pulses on the target ion possessing different rotation angles (that is, lengths of Rabi pulses) about different rotation axes (that is, phases of the exciting radiation), see Table 1. Together with two carrier $\pi/2$ -pulses

(Ramsey pulses) before and after this sequence, this completes the single-ion CNOT gate operation.

Individual ion addressing and read-out

For detection of the internal quantum states, we excite the $S_{1/2}$ to $P_{1/2}$ dipole transition³ near 397 nm and monitor the fluorescence with an intensified charge-coupled device (CCD) camera separately for each ion. Fluorescence indicates that the ion was in the $S_{1/2}$ state; no fluorescence reveals that it was in the $D_{3/2}$ state. By repeating the experimental cycle 100 times we find the average state populations. Fluorescence is collected with the CCD camera for 23 ms (data of Fig. 1) and 10 ms (all other data). The fluorescence intensity is integrated over an area of approximately $3\mu\text{m} \times 3\mu\text{m}$ around the ions by binning the corresponding pixels of the enlarged image on the CCD camera. Thus, state detection of each qubit is performed with an efficiency of about 98% with the residual error of about 2% resulting from spurious fluorescence light of the adjacent ion (cross-talk) or in the case of the 23 ms collection time, from spontaneous decay.

Individual state manipulation of the ions is performed with a tightly focused laser beam near 729 nm. The inter-ion distance is $5.3\mu\text{m}$ and the gaussian beam width (full-width at half-maximum, FWHM, at the focus) is $2.5\mu\text{m}$. Directing the beam onto one ion, the remaining intensity in the wing of the beam incident on the neighbouring ion is suppressed by a factor of 2.5×10^{-3} . The addressing beam can be switched from one ion to the other within $15\mu\text{s}$ using an electro-optical beam deflector.

Received 18 December 2002; accepted 17 February 2003; doi:10.1038/nature01494.

1. Cirac, J. I. & Zoller, P. Quantum computations with cold trapped ions. *Phys. Rev. Lett.* **74**, 4091–4094 (1995).
2. Nägler, H. C. *et al.* Laser addressing of individual ions in a linear ion trap. *Phys. Rev. A* **60**, 145–148 (1999).
3. Nägler, H. C. *et al.* Investigating a qubit candidate: Spectroscopy on the $S_{1/2}$ to $D_{3/2}$ transition of a trapped calcium ion in a linear Paul trap. *Phys. Rev. A* **61**, 023405 (2000).
4. Häffner, H. *et al.* Precision measurement and compensation of optical Stark shifts for an ion-trap quantum processor. *Phys. Rev. Lett.* (in the press); preprint available at (<http://arXiv.org/abs/physics/0212040>) (2002).
5. Childs, A. M. & Chuang, I. M. Universal quantum computation with two-level trapped ions. *Phys. Rev. A* **63**, 012306 (2001).
6. Levitt, M. H. Composite pulses (NMR spectroscopy). *Prog. Nucl. Magn. Reson. Spectrosc.* **18**, 61–122 (1986).
7. DiVincenzo, D. P. The physical implementation of quantum computation. *Fortschr. Phys.* **48**, 771–783 (2000).
8. Sleator, T. & Weinfurter, H. Realizable universal quantum logic gates. *Phys. Rev. Lett.* **74**, 4087–4090 (1995).
9. DiVincenzo, D. P. Two-bit gates are universal for quantum computation. *Phys. Rev. A* **51**, 1015–1022 (1995).
10. Shor, P. W. in *Proc. 35th Annu. Symp. Foundations of Computer Science* (ed. Goldwasser, S.) 124–133 (IEEE Computer Society Press, Los Alamitos, California, 1994).
11. Vandersypen, L. M. K. *et al.* Experimental realization of Shor's quantum factoring algorithm using nuclear magnetic resonance. *Nature* **414**, 883–887 (2001).
12. Šašura, M. & Žužek, V. Cold trapped ions as quantum information processors. *J. Mod. Opt.* **49**, 1593–1647 (2002).
13. Roos, Ch. *et al.* Quantum state engineering on an optical transition and decoherence in a Paul trap. *Phys. Rev. Lett.* **83**, 4713–4716 (1999).
14. Meekhof, D. M., Monroe, C., King, B. E., Itano, W. M. & Wineland, D. J. Generation of nonclassical motional states of a trapped atom. *Phys. Rev. Lett.* **76**, 1796–1799 (1996).
15. Demhelt, H. Proposed $10^{14}\Delta\nu > \nu$ laser fluorescence spectroscopy on Ti^+ mono-ion oscillator. *Bull. Am. Phys. Soc.* **20**, 60 (1975).
16. Turchette, Q. A. *et al.* Deterministic entanglement of two trapped ions. *Phys. Rev. Lett.* **81**, 3631–3634 (1998).
17. Sackett, C. A. *et al.* Experimental entanglement of four particles. *Nature* **404**, 256–259 (2000).
18. Monroe, C., Meekhof, D. M., King, B. E., Itano, W. M. & Wineland, D. J. Demonstration of a fundamental quantum logic gate. *Phys. Rev. Lett.* **75**, 4714–4717 (1995).
19. Gulde, S. *et al.* Implementation of the Deutsch–Jozsa algorithm on an ion-trap quantum computer. *Nature* **421**, 48–50 (2003).
20. Rohde, H. *et al.* Sympathetic ground state cooling and coherent manipulation with two-ion crystals. *J. Opt. B* **3**, S34–S41 (2001).
21. Jones, J. A. Robust Ising gates for practical quantum computation. *Phys. Rev. A* **67**, 012317 (2003).
22. de Vivie-Riedle, R., Rabitz, H. & Kompa, K. (eds) *Chem. Phys.*, **267**, Issues 1–3 (2001). Special issue on coherent control.
23. Pan, J.-W., Bouwmeester, D., Daniell, M., Weinfurter, H. & Zeilinger, A. Experimental test of quantum nonlocality in three-photon Greenberger–Horne–Zeilinger entanglement. *Nature* **403**, 515–519 (2000).
24. Steane, A. M. Efficient fault-tolerant quantum computing. *Nature* **399**, 124–126 (1999).
25. Duan, L. M., Lukin, M., Cirac, J. I. & Zoller, P. Long-distance quantum communication with atomic ensembles and linear optics. *Nature* **414**, 413–418 (2001).

Acknowledgements We thank P. Zoller for discussions and we gratefully acknowledge support by the European Commission (QUEST and QUBITS networks), by the Austrian Science Fund (FWF), and by the Institut für Quanteninformation GmbH. H.H. is supported by the Marie-Curie programme of the European Commission.

Competing interests statement The authors declare that they have no competing financial interests.

Correspondence and requests for materials should be addressed to R.B. (e-mail: Rainer.Blatt@uibk.ac.at).